Probing the Selectivity and Activity of Palladium-Catalysts for Enantioselective β-C(sp³)-H Bond Arylation Reactions

Erik A. Romero[1], Gang Chen[2], Milan Gembicky[1], Rodolphe Jazzar[1], Jin-Quan Yu*[2], Guy Bertrand*[1]

[1] UCSD-CNRS Joint Research Laboratory (UMI 3555), Department of Chemistry and Biochemistry, University of California, San Diego, La Jolla, California 92093-0358, United States

[2] Department of Chemistry, The Scripps Research Institute, 10550 N. Torrey Pines Road, La Jolla, California 92037, United States

Supporting Information Placeholder

ABSTRACT: Chiral acetyl-protected aminoethyl quinoline (APAQ) ligands were recently discovered to afford highly active and enantioselective palladium catalysts for the arylation of methylene C(sp³)-H bonds. Herein, we investigate the origins of these heightened properties through a combination of density functional theory (DFT), X-ray crystallography, and detailed analyses of topological steric maps as strategic tools for predicting chiral inductive effects imparted on the transition-metal center by ancillary ligand scaffolds. DFT and single crystal X-ray diffraction studies both confirm the existence of an unusual amide-bridged dimerization motif of catalytically active APAQ-Pd complexes. Comparison of the structural parameters of these complexes to those featuring acetyl-protected aminoethyl pyridine (APAPy) as ligand confirms that the high activity of APAQ-Pd complexes originates from the presence of the quinoline ring, which serves to promote dissociation of catalytically inactive palladium dimers. Furthermore, analysis of the steric topographic maps for a representative subset of monomeric, monoligated palladium complexes allowed us to draw a unique parallel between the 3-dimensional structures of these catalysts and their reported asymmetric induction in β-C-(sp³)-H bond arylation reactions. Finally, we identified cooperative non-covalent interactions present between the APAQ ligand and the substrate as a crucial factor for imparting bias between the two chemically equivalent methylenic C(sp³)-H bonds prior to CMD activation.

INTRODUCTION

Discoveries over the past 40 years have allowed the functionalization of unreactive C-H bonds through transition metal-catalyzed processes to produce structurally diverse organic molecules.[1] More recently, these advances have been applied to the development of organometallic complexes capable of controlling the site- and stereospecificity of both intra- and inter-molecular C-H bond transformations.[2] Despite these significant advancements, the regio- and enantioselective catalytic functionalization of aliphatic C(sp³)-H bonds remains a significant challenge due to the difficulty associated in differentiating between two geminal hydrogen atoms.[3] The use of directing groups represents the most successfully implemented strategy to control aliphatic C-H bond functionalization reactions.[4]

Amide moieties derived from carboxylic acids constitute one such class of directing groups that have afforded exceptional regio- and enantioselective control in transforming proximal C-H bonds into a broad range of synthetically useful functional groups.[5] Exploiting this strategy, one of us reported a number of Pd-catalyzed processes for the functionalization of β-C(sp³)-H bonds.[6] More recently, these methodologies were extended to the stereoselective arylation of unbiased β-methylene C(sp³)-H bonds by combining a novel acetyl-protected aminoethyl quinoline (^{Et}APAQ) ligand with palladium-acetate. (Figure 1).[7] This catalyst tolerates a broad array of sterically and electronically diverse aryl-iodide reagents and affords the arylated products in excellent enantiometic excesses (ee's).

In a collaborative effort with Houk *et al.*,[8] one of us recently reported a detailed computational investigation of the mechanism involves in the Pd-catalyzed β-C-H bond arylation reaction, which is briefly summarized in Figure 1. It was determined that $Pd(OAc)_2$ reacts with the APAQ ligands to form a reactive mono-ligated palladium-acetate complex **A**. It was also proposed that the thermodynamically favorable off-cycle palladium dimer **B** is not an active catalytic species, but rather exists as the resting-state of the catalytic cycle. From **A**, a substrate molecule can be metalated by extrusion of AcOH thus affording complex **C**, which features a favorable agostic C(sp)-H interaction. The ensuing concerted metalation deprotonation (CMD) step affords complex **D** that can oxidatively add an aryl-iodide to generate a transient Pd(IV) intermediate (not shown), prior to reductive elimination of the product.

Subsequent reaction with silver(I)-salts and HOAc was proposed to regenerate the un-ligated $Pd(OAc)_2$ starting material thus closing the catalytic cycle.

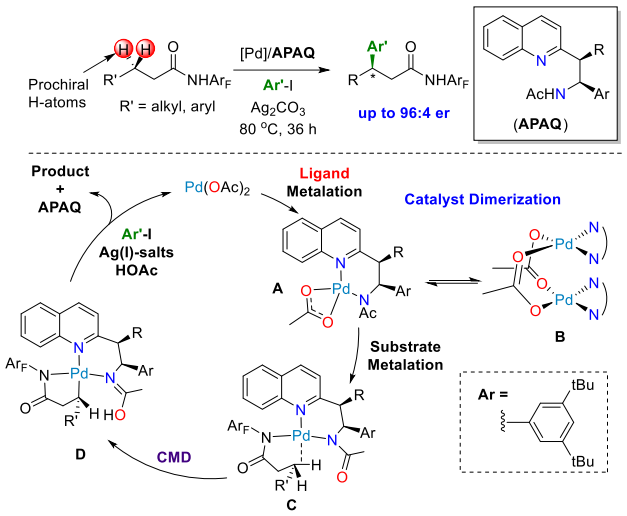

Figure 1. APAQ/Pd complexes catalyze the enantioselective arylation of C-H bonds located beta to a carbonyl. Recent mechanistic investigations, employing DFT, identified this sequence of elementary reaction steps as key in forming β-arylated products.

Herein, we investigate the coordination of APAQ ligands to palladium and report a highly unusual binding motif for Pd(II) dimers. We extend the use of topological steric maps as a strategic tool to predict potential chiral inductive effects. Finally, using these data in conjunction with those obtained during catalytic reactions, we attempt to understand the origin of the selectivity and activity of APAQ/Pd catalysts in the arylation of β-C(sp^3)-H bonds.

COMPUTATIONAL DETAILS

All calculations were carried out using the Gaussian 09 program suite.[9] Geometry optimizations were performed with the B3LYP functional.[10] The Def2-TZVP basis set[11] with ECP was used for Pd and the 6-31G(d,p) basis set[12] was used for all other atoms. Frequency calculations at the same level of theory were performed to identify the number of imaginary frequencies (zero for local minima) and to provide the thermal corrections for Gibbs free energy determinations. Due to the lack of dispersion in the B3LYP functional, dispersion correction calculations using the corresponding B3LYP-D functional were performed with the DFT-D3 program of Grimme.[13] The relative Gibbs free energies (at 298.15 K) are given in kcal/mol and are illustrated using CYLView.[14]

RESULTS AND DISCUSSION

Computational Analysis of ^{H}APAPy and APAQ Ligated Palladium Dimers Using DFT. Acetate-bridged Pd(II) dimers featuring a wide variety of bidentate chelating ligands are reported in the literature.[15] Using density functional theory, we investigated whether similar dimeric motifs were possible using the ^{H}APAPy ligand (Figure 2) as a simplified model for the APAQ ligands. In line with literature precedents, the thermodynamic minimum for acetate-bridged dimer **1a** was located; however, due to the steric hindrance imposed by the bulky 3,5-di-tert-butylbenzene aryl group alpha to the amide fragment, we wondered whether alternative dimerization modes could be envisaged. Capitalizing on the Lewis basic amide oxygen atom, we uncovered the amide-bridged palladium dimer **1b** as a significantly more favorable alternative to **1a** (ΔG = -33.3 kcal/mol), probably because of the unfavorable steric interactions between the 3,5-di-tert-butylphenyl groups. Note that the Pd-Pd bond distance is predicted to be much shorter in **1b** than in **1a**, which can be further attributed to the alleviation of steric repulsion.

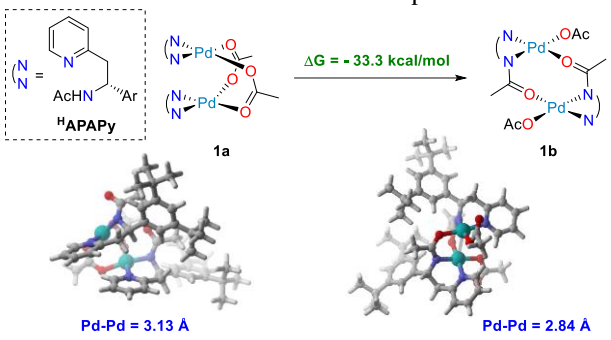

Figure 2. Comparing the thermodynamic favorability of acetate- versus amide-bridged palladium dimers ligated by ^{H}APAPy. Aryl: 3,5-di-tert-butylphenyl.

Turning our attention to the larger APAQ ligand scaffold, we located the thermodynamic minima corresponding to the acetate-bridged dimers **2a** and **3a** as well as the amide-bridged dimers **2b** and **3b** (Figure 3). In contrast to **1a** and **1b**, these APAQ ligated complexes exhibit significantly longer Pd-Pd distances (**2a**: 3.63 Å, **2b**: 3.59 Å, **2b**: 3.19 Å, and **3b**: 3.23 Å), which is a testament of the steric bulk imparted by the quinoline ring. From the optimized geometries of **2a** and **3a**, it is clear that unfavorable C(sp^2)-H to π interactions arising from the orthogonal orientation of the quinoline rings (highlighted with a red box) causes the extreme lengthening of the Pd-Pd distance. To alleviate these destabilizing steric interactions, complexes **2** and **3** would only exist as amide-bridged dimers because these C(sp^2)-H to π interactions are replaced with stabilizing π- π interactions and a sufficiently close Pd-Pd distance to suggest a partial overlap of the dz^2 orbitals from both palladium centers. We found that the re-orientation of **2a** to **2b** and **3a** to **3b**, like complex **1**, are also highly exothermic processes (ΔG = -35.9 and -34.7 kcal/mol, respectively).

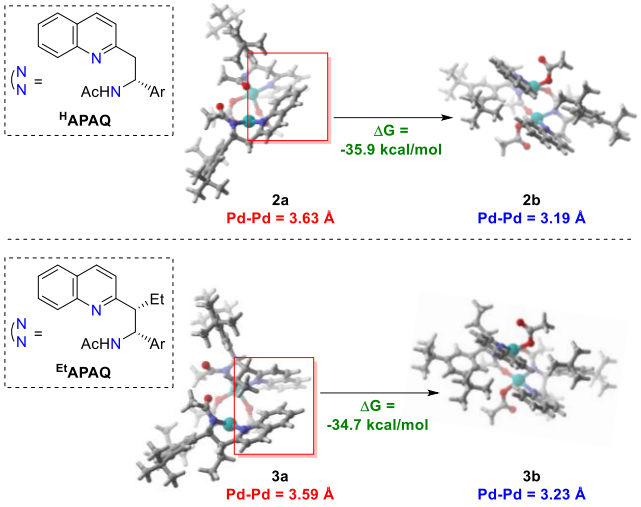

Figure 3. APAQ-ligated palladium dimers feature long Pd-Pd distances due to the unfavorable steric repulsion of the quinoline rings. Alkylation of the benzylic methylene group forces the dissociation of OAc-bridged dimers for ^{Et}APAQ. Both APAQ-ligated palladium complexes favor formation of amide-bridged dimeric species. Aryl: 3,5-di-tert-butylphenyl.

Preparation of Palladium Complexes 1, 2, and 3. Intrigued by these computational data, we set out to investigate the nature of the Pd intermediates formed upon reaction of ^{H}APAPy, ^{H}APAQ, and ^{Et}APAQ with $Pd(OAc)_2$. Reaction of ^{H}APAPy with equimolar $Pd(OAc)_2$ in $CHCl_3$ at 40 °C led to the formation of a single organometallic species that was confirmed to feature an amide-bridged binding motif by a single crystal X-ray diffraction study (**1**, Figure 4).

Complex **1** crystallized in the $P2_1$ space group with one molecule in the asymmetric unit cell. The solid-state structure exhibits a short distance between the two Pd centers (2.87 Å), which is very similar to the value predicted by DFT (2.84 Å). This value is well within the sum of the Van der Waals radii for a bonding interaction between two Pd atoms (3.26 Å).

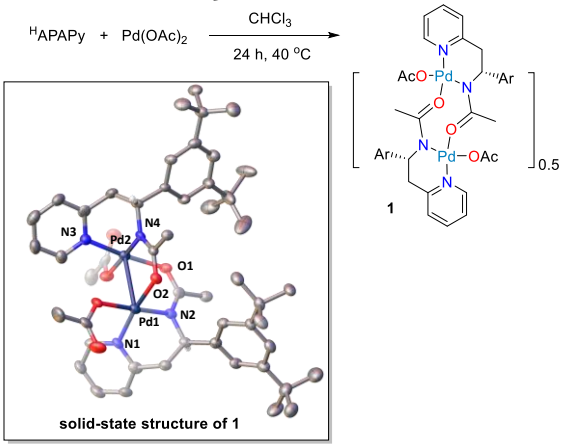

Figure 4. Preparation and solid-state structure of **1**. Hydrogen atoms not located at chiral centers, solvent, and positional disorder have been omitted for clarity. Thermal ellipsoid parameters are set at 50% probability. Selected distances (Å) and angles (°): Pd1-N1 1.995(7); Pd1-N2 2.013(7); O1-Pd2 2.038(7); Pd2-N3 2.003(8); Pd2-N4 2.000(7); O2-Pd1 2.040(6); Pd1-Pd2 2.8734(9); N1-Pd1-N2: 86.3(3); and N3-Pd2-N4: 86.7(3).

Encouraged by this result, we turned our attention to the reaction of ^{H}APAQ and ^{Et}APAQ with $Pd(OAc)_2$. To our surprise, under reaction conditions similar to those used for ^{H}APAPy ($CHCl_3$, 40 °C), a mixture of products was observed by ^{1}H NMR spectroscopy. Performing the reaction in the presence of a sacrificial amine base afforded complexes **2** and **3** in 73 and 27% yield, respectively, after re-crystallization (Scheme 1).

Scheme 1. Reaction of APAQ ligands with $Pd(OAc)_2$ in the presence of a sacrificial amine base affords the dimeric bimetallic $[LPd(OAc)]_2$ complexes 2 and 3. Aryl: 3,5-di-tert-butylphenyl.

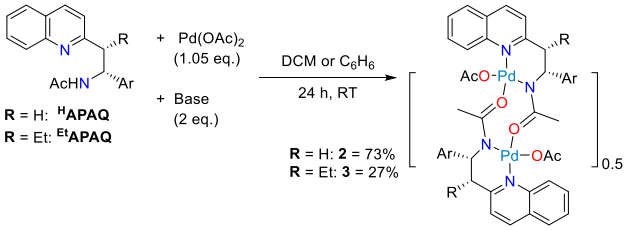

Complexes **2** and **3** were characterized by a single-crystal X-ray diffraction study. As in the case of complex **1**, both **2** and **3** also exhibit a dimeric amide-bridged motif in the solid-state (Figure 5). Complex **2** crystallized in the $P2_12_12$ space group whereas **3** crystallizes in the C2 space group. The distances between the two palladium centers in these complexes are significantly longer than in **1** and are only slightly below the sum of the Van der Waals radii (3.20 Å for **2** and 3.23 Å for **3**). Here again, the Pd-Pd distances are in line with those predicted by DFT.

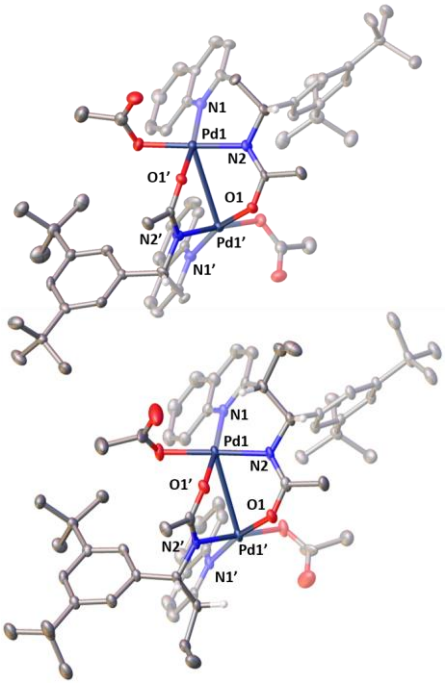

Figure 5. Solid-state structures of **2** (top) and **3** (bottom). Hydrogen atoms not located at chiral centers, solvent, and positional disorder have been omitted for clarity. Thermal ellipsoid parameters are set at 50% probability. Complexes **2** are crystallographically symmetric and can be described by the operators 1-X,1-Y,+Z and 1-X,+Y,1-Z, respectively. Selected distances (Å) and angles (°): **2**: Pd1-N1: 2.022(4); Pd1-N2: 2.023(4); O1-Pd1' 2.027(4); Pd1-Pd1' 3.1951(10); and N1-Pd1-N2: 90.0(2). **3:** Pd1-N1 2.024(4); Pd1-N2 2.027(3); O1-Pd1' 2.021(3); Pd1-Pd1' 3.2290(8); and N1-Pd1-N2: 89.10(4).

Importance of the Quinoline Ring on Catalytic Activity. We previously reported that the APAQ ligand scaffold generates highly active Pd-catalysts for β-C-(sp³)-H bond arylation reactions. In fact, providing the right substitution pattern on the ligand backbone, these ligands have achieved exceptional enantioselectivity/control (Figure 6).[7] Unlike APAQ ligands, catalysts featuring the pyridine based ^{H}APAPy ligands have been shown to be significantly less active only yielding β-arylated products in 28% yield after 36 hours (**VI**).[8]

This result could tentatively be rationalized by considering the Pd-Pd distance in complexes **1** (2.87 Å), **2** (3.20 Å), and **3** (3.23 Å), which suggest that complex **1** is more stable and thereby less prone to dissociation in solution than complexes **2** and **3**. In light with the catalytic activity, this unfavorable bond dissociation could indicate that ^{H}**APAPy**-ligated palladium complex **1** primarily lies in its dimeric form, which serves as a resting state for the catalytic cycle. This hypothesis is further supported by the fact that the ^{H}APAQ palladium complex **2** could be isolated as a monomer $\mathbf{2}_{mono}$ (Figure 7, bottom trace) and was found to dimerize only after extended periods of time in concentrated solutions.[16] The ^{1}H NMR spectrum of $\mathbf{2}_{mono}$ invariably contained traces of the more thermodynamically stable dimeric species **2**, resonances from which can be clearly observed and have been labeled by orange triangles in Figure 7. This phenomenon was not observed during the preparation of the amide-bridged dimer **1;** the ^{1}H NMR spectrum only shows signals of the latter (top trace). All together, these data and observations clearly show that the significant differences observed in the activities for these two ligand classes arise from the presence of the quinoline ring on the **APAQ** scaffold, which likely prevents the formation of the off-cycle palladium dimers **B**.

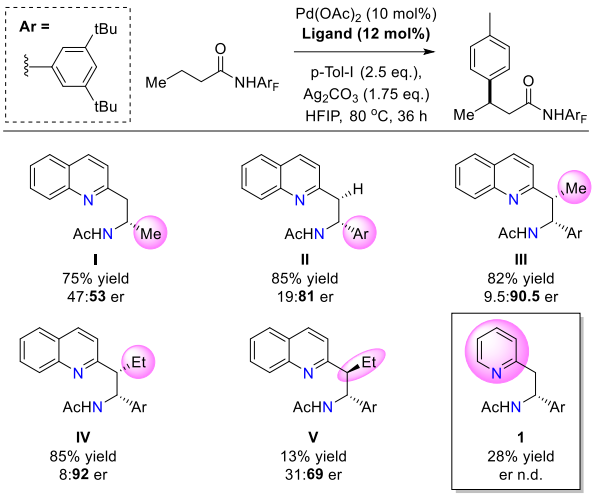

Figure 6. Selected ligands that were surveyed with palladium for activity in β-C-H bond arylation reactions along with their isolated product yields and the observed enantiomeric ratios.

Correlating Enantioselectivity With Ancillary Ligand Structure Using Steric Topographical Analysis. We next wondered if we could draw a parallel between the 3-dimensional structures of these catalysts and their reported asymmetric induction in β-C-(sp³)-H bond arylation reactions (Figure 6).[7] Asymmetric catalysis relies on the ability of ancillary ligands to strategically block specific sections of the coordination sphere in order to transfer asymmetric information from the catalyst to the substrate. Thus, we hypothesized that topological steric maps,[17,18] obtained from a representative subset of monomeric, monoligated palladium complexes $\mathbf{I}_{mono}$-$\mathbf{V}_{mono}$ and $\mathbf{1}_{mono}$ (Figure 8), could afford key insights into the rational design of novel ligand scaffolds for use in asymmetric reaction development. Note that to facilitate this discussion, the steric maps presented in Figure 8 have been partitioned into 4 quadrants.

We first considered $\mathbf{1}_{mono}$ and $\mathbf{I}_{mono}$, two ligand systems unable to induce appreciable enantio-enrichment under catalytic conditions. In either environment, significant steric occupancy is only displayed in a single quadrant from the C_6H_3(o-^{t}Bu)$_2$ moiety in $\mathbf{1}_{mono}$(SE), or from the quinoline moiety in $\mathbf{I}_{mono}$ (NW). For comparison, $\mathbf{II}_{mono}$, which combines the steric effect of the C_6H_3(o-^{t}Bu)$_2$ and the quinoline in their respective opposing quadrants, has been shown to afford significant enantio-induction (19:81 er). This suggests that the chiral scaffold can be accurately modeled by a quadrant diagram where the NW and SE quadrants are sterically congested forcing the substrates to reside in the less occupied NE and SW quadrants.

Catalytic studies involving $\mathbf{III}_{mono}$-$\mathbf{V}_{mono}$ highlighted the importance of a strategic substitution pattern on the APAQ ligand backbone. These groups, which reside in the SW quadrant of their respective plots, appear to have a more nuanced effect on the asymmetric transformation. To further investigate the role of the ethyl group on the stereochemical determining step of the catalytic cycle, we examined the optimized 3D model of complex $\mathbf{IV}_{sub}$, that

is bound to a model substrate, to determine whether non-covalent interactions between the APAQ ligand and the substrate could be responsible for imparting bias between the methylene C(sp³)-H bonds prior to cyclopalladation (Figure 9). Such hydrogen bonding interactions are well known to promote high er's for asymmetric catalytic reactions occurring in the catalytic pockets of enzymes.[19] In our case, we determined that complex **IV$_{sub}$** exhibits a strong arene π-stacking interaction of the fluorinated auxiliary with the quinoline ring (π-π distance ~3.1 Å). Surprisingly, we observed a hydrogen bonding interaction between an ortho-fluorine atom on the amide auxiliary ring and a hydrogen atom from the ethyl group in both (R)-**IV$_{sub}$** and (S)-**IV$_{sub}$** (H--F distance: 2.2 Å) well within the sum of the Van der Waals radii for a hydrogen atom (120 pm) and a fluorine atom (135 pm). The presence of these interactions suggests that the ethyl group could serve to immobilize the substrate amide auxiliary fragment throughout the carbopalladation process.

Having considered the role of the alkyl groups on the backbone of the APAQ ligand, we also looked for other interaction that could impart sufficient bias on the methylene group so as to favor reaction at one geminal C(sp³)-H bond over the other. From a thermodynamic point of view, the two conformations (R)-**IV$_{sub}$** and (S)-**IV$_{sub}$** only differ in Gibbs free energy by 0.10 kcal/mol in favor of (S)-**IV$_{sub}$**, which cannot alone support the observed S enantioselectivity induced by this ligand diastereomer under catalytic conditions. Upon further analysis of the optimized geometries, we noticed hydrogen bonding interactions in both the (R)-**IV$_{sub}$** and (S)-**IV$_{sub}$** conformers between the substrate alkyl chain and the ligand amide oxygen atom. For the (R)-**IV$_{sub}$** configuration, there is a distinct interaction with the β-C(sp³)-H hydrogen atom (2.41 Å), supporting a concerted process between this C-H bond, the amide, and the metal. Conversely, the (S)-**IV$_{sub}$** configuration shows hydrogen bonding between the terminal methyl group of the substrate and the amide fragment (2.48 Å). We believe that despite (R)-**IV$_{sub}$** exhibiting a CMD-like interaction with the C(sp³)-H bond, this configuration also leads to an unfavorable arrangement of the terminal CH_3 moiety in the more sterically congested southern hemisphere of the coordination sphere (Figure 8). Moreover, the terminal CH3 hydrogen bonding interaction observed in (S)-**IV$_{sub}$** could help in locking the β-C(sp³)-H hydrogen atom in the desired configuration.

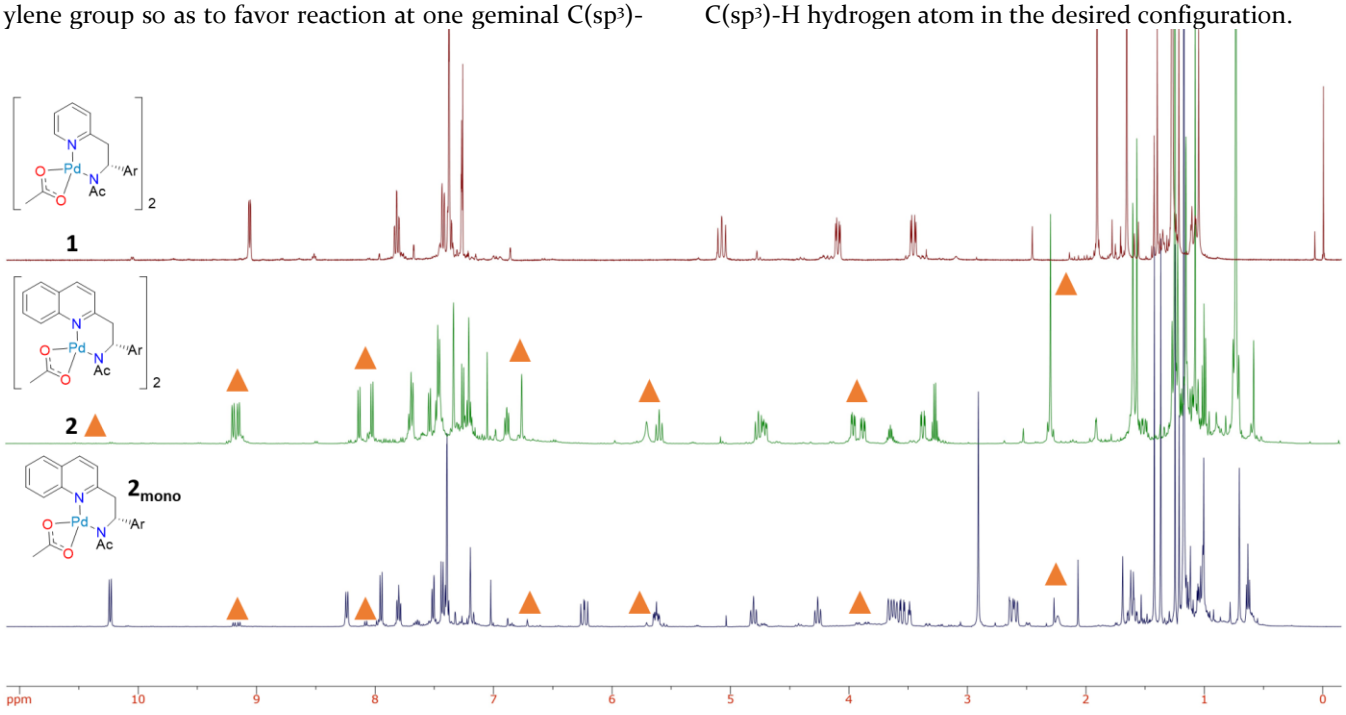

Figure 7. ^{H}APAQ-ligated palladium form complex **2** (center trace). A low concentration of the dimeric species **2** is visible in the spectrum of **2$_{mono}$** (select resonances for dimer **2** are indicated by orange triangles). Only one species exists for the reaction of ^{H}APAPy and $Pd(OAc)_2$ (top trace), which is the dimeric product **1**. Aryl: 3,5-di-tert-butylphenyl.

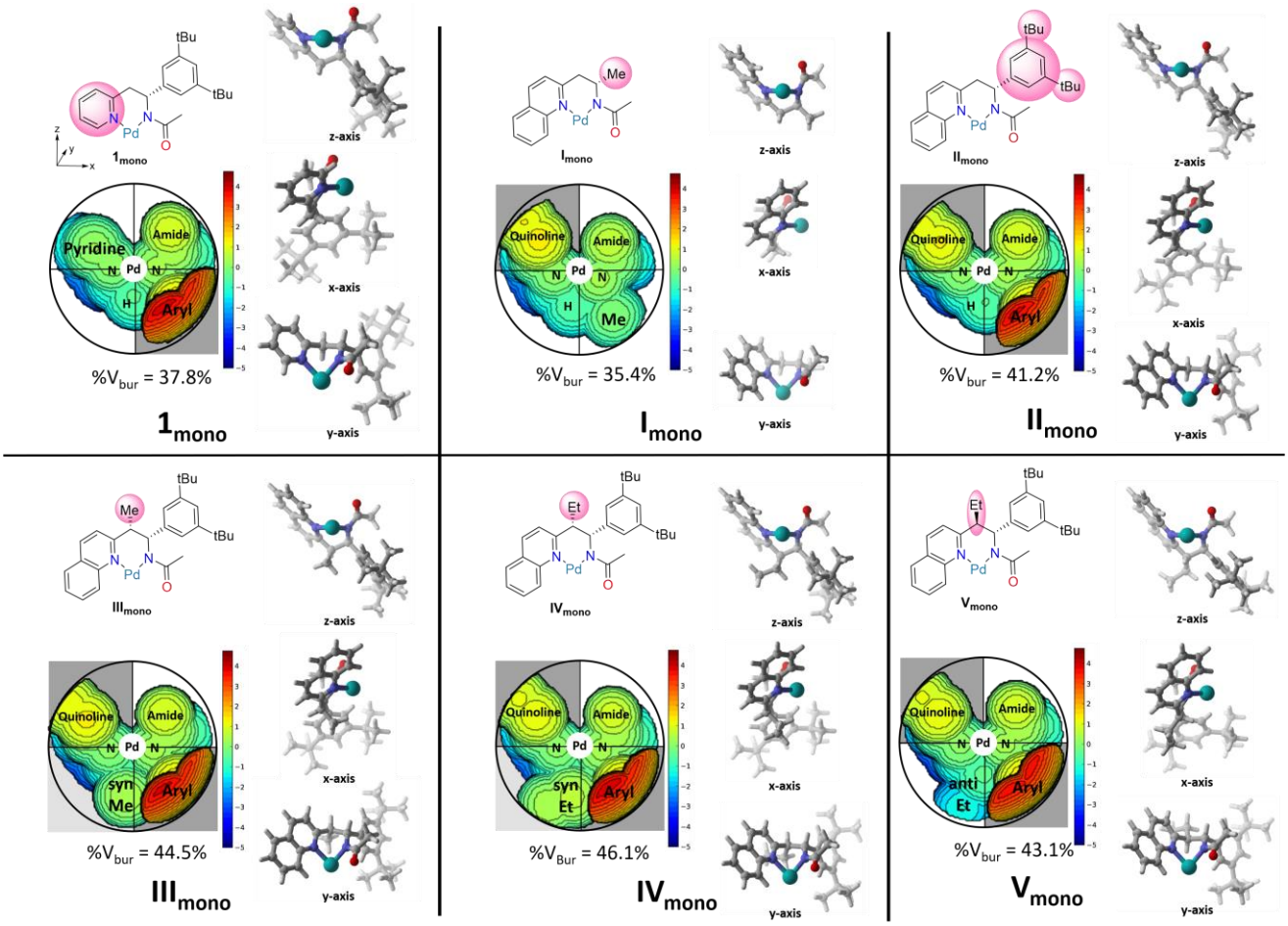

Figure 8. Steric topology maps for monomeric complexes $\mathbf{I}_{mono}$-$\mathbf{V}_{mono}$ and $\mathbf{1}_{mono}$. Each complex is along each of the 3 axes to clearly depict the steric contributions of the ligand. Aryl: 3,5-di-tert-butylphenyl.

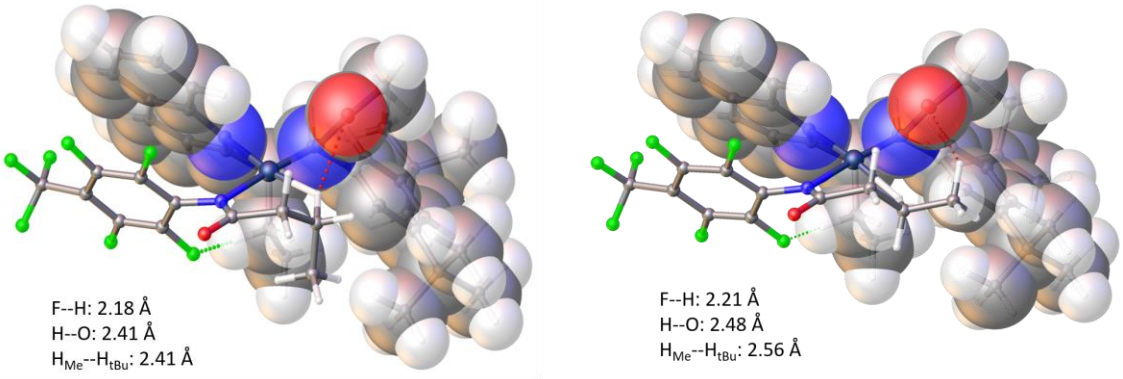

Figure 9. Comparison of the non-covalent interactions existing between APAQ ligand and the substrate. This analysis clearly depicts the role of the alkyl group as a hydrogen bond donor to the fluorinated auxiliary.

CONCLUSION

Herein, we have disclosed the preparation, isolation, and crystallographic characterization of APAPy- and APAQ-ligated palladium complexes, the latter of which exhibit excellent activity and enantioselectivity in β-C-(sp^3)-H bond arylation reactions. In contrast to other Pd(II) dimers, we found that these bulky chelating ligands favor an unusual amide-bridged dimerization motif because this binding mode better alleviates unfavorable steric repulsion of the ligands while simultaneously incorporating favorable Pd-Pd bonding interactions. From these studies, we determined that the origin of the high catalytic activities with APAQ ligands should be attributed to the presence of the quinoline ring. This heterocycle promotes the dissociation of the off-cycle palladium di-

mers to their corresponding monomers, which effectively increases the solution-phase lifetime of catalytically active monomeric palladium complexes.

Since its development in 2016, steric topographic maps have been used primarily to determine the buried volume of a given ligand or to visualize the steric environment around a metal center ligated by a chiral molecule. Here, using the β-C-(sp^3)-H bond arylation as a model reaction, we show that the combination of DFT and steric maps could be used as a predictive tool.

EXPERIMENTAL SECTION

General Considerations. All manipulations were carried out under aerobic conditions unless otherwise noted. Starting materials and solvents of reagent-grade were purchased from commercial suppliers and used as received without further purification. Solution-phase ^{1}H and ^{13}C NMR spectra were recorded on a Varian Inova 500 MHz spectrometer. All NMR signals are reported in ppm relative to $SiMe_4$ with reference to the residual solvent resonances of C_6D_6 (7.16 ppm for ^{1}H and 128.06 ppm for ^{13}C) and $CDCl_3$ (7.26 ppm for ^{1}H and 77.16 ppm for ^{13}C). NMR multiplicities are denoted as follows: s = singlet, d = doublet, t = triplet, q = quartet, quin = quintet, m = multiplet, and br = broad. Ligands $\mathbf{L_1}$ and $\mathbf{L_2}$-$\mathbf{L_3}$ were prepared according to literature procedures.

Synthesis of complex 1. A 10 mL scintillation vial was charged with ^{H}APAPy ligand $\mathbf{L_1}$ (35.2 mg, 99.4 μmol, 1 equiv.), $Pd(OAc)_2$ (22.3 mg, 99.4 μmol, 1 equiv.), and 2 mL chloroform. The resulting solution was stirred at 40 °C for 24 hours, at which point, all volatiles were evaporated under vacuum. The residue was extracted with 2 x 2 mL benzene, filtered through a pipette plug of celite, and concentrated under vacuum to afford complex **1** as a light-orange powder in 98% yield (50.7 mg). Single crystals suitable for an X-ray diffraction study were grown by vapor diffusion of diethyl ether into a saturated dichloromethane solution at room temperature. M.P. xxxxx °C dec. ^{1}H NMR ($CDCl_3$, 500 MHz): δ 0.95 (s, 9H), 1.40 (s, 9H), 1.84 (s, 3H), 2.35 (s, 3H), 2.65 (s, 3H), 3.36-3.45 (m, 4H), 4.28 (dd, *J* = 14.34, 6.76 Hz, 1H), 4.48 (t, J = 8.71 Hz,1H), 4.81 (m, 1H), 5.19 (d, J = 10.70 Hz, 1H), 5.56 (s, 1H), 6.37 (d, J = 7.58 Hz, 2H), 6.55 (d, J = 7.09 Hz, 1H), 6.70 (t, J = 7.39 Hz, 1H), 6.77 (t, J = 7.19 Hz, 1H), 6.93-6.99 (m, 3H), 7.43 (d, J = 7.69 Hz, 1H), 8.59 (d, J = 10.67 Hz, 1H). ^{13}C NMR ($CDCl_3$, 125 MHz): δ 9.7, 22.4, 27.2, 29.3, 29.4, 31.1, 42.7, 62.7, 77.4, 80.9, 124.8, 129.8, 134.1, 145.1, 168.3, 250.9. HRMS ESI-TOF+ found m/z = xxxxxxx, [M + H]+ calculated for [C25H35N2O3Pd]+ m/z = 517.1677.

Synthesis of complex 2. Charge a 20 mL scintillation vial with ligand $\mathbf{L_2}$ (40 mg, 99.4 μmol, 1 equiv.) and $Pd(OAc)_2$ (22.3 mg, 99.4 μmol, 1 equiv.) and a magnetic stir bar. Add 1 mL dichloromethane and stir until fully dissolved. Add *N*-methylmorpholine (16.3 μL,149.2 μmol, 1.5 equiv.). Stir resulting solution overnight followed by filtration through a plug of celite. Wash the celite plug with 2 mL dichloromethane. The combined organic layers were evaporated under vacuum resulting in an oily residue. Pentane (5 mL) was added to the residue and then stirred for 10 minutes at room temperature. The solid precipitate was collected by vacuum filtration and dried under vacuum yielding crude **2** as a light-yellow powder. The title compound was purified by recrystallization from a mixture of diethyl ether and dichloromethane in 73% yield (41.1 mg). Single crystals suitable for an X-ray diffraction study were grown by vapor diffusion of diethyl ether into a saturated dichloromethane solution at room temperature. M.P. xxxxx °C dec. ^{1}H NMR ($CDCl_3$, 500 MHz): δ 0.72 (s, 18H), 1.07 (s, 3H), 1.15 (s, 3H), 1.24 (s, 18H), 1.59 (s, 3H), 2.29 (s, 3H), 3.36 (dd, *J* = 14.1, 3.8 Hz, 1H), 3.87 (dd, *J* = 13.6, 4.5 Hz, 1H), 3.95 (dd, *J* = 11.9, 3.7 Hz, 1H), 4.70 (dd, *J* = 12.3, 4.3 Hz, 1H), 4.75 (t, *J* = 12.9 Hz, 1H), 5.59 (t, *J* = 12.9 Hz, 1H), 5.70 (s, br, 1H), 6.75 (s, 1H), 6.88 (t, *J* = 7.9 Hz, 1H), 7.20 (s, 2H), 7.25 (d, *J* = 8.2 Hz, 1H), 7.32 (s, 2H), 7.46 (m, 4H), 7.53 (d, *J* = 8.2 Hz, 1H), 7.68 (t, *J* = 8.9 Hz, 2H), 8.01 (d, *J* = 8.3 Hz, 1H), 8.13 (d, *J* = 8.3 Hz, 1H), 9.17 (dd, *J* = 22.1, 8.7 Hz, 2H). ^{13}C NMR ($CDCl_3$, 125 MHz): δ 15.4, 21.3, 21.6, 23.7, 25.1, 31.2, 31.7, 34.6, 35.3, 51.4, 51.5, 56.6, 61.1, 66.0, 120.3, 120.4, 121.1, 121.2, 121.4, 121.5, 127.4, 127.5, 127.6, 127.8, 127.8, 127.9, 127.9, 128.4, 130.6, 131.8, 139.9, 140.1, 141.9, 143.5, 146.5, 147.3, 150.1, 151.6, 160.3, 161.7, 174.7, 176.3, 181.0. HRMS ESI-TOF+ found m/z = 567.1860, $[M + H]^+$ calculated for $[C_{29}H_{37}N_2O_3Pd]^+$ m/z = 567.1845.

Synthesis of complex $\mathbf{2_{mono}}$. Charge a 20 mL scintillation vial with ligand $\mathbf{L_2}$ (40 mg, 99.4 μmol, 1 equiv.) and $Pd(OAc)_2$ (22.3 mg, 99.4 μmol, 1 equiv.) and a magnetic stir bar. Add 1 mL benzene and stir until fully dissolved. Add *N*-methylmorpholine (16.3 μL,149.2 μmol, 1.5 equiv.). Stir resulting solution overnight followed by filtration through a plug of celite. Wash the celite plug with 2 mL dichloromethane. The combined organic layers were concentrated to 1 mL and triturated with pentane (5 mL) and stirred for 10 minutes at room temperature. The solid precipitate was collected by vacuum filtration and dried under vacuum yielding $\mathbf{2_{mono}}$ (containing traces of **2**) as a light-yellow powder. **N.B.**: $[NMMH]^+[OAc]^-$ present in the sample and could only be successfully removed by crystallizing $\mathbf{2_{mono}}$; however, all attempts to crystallize $\mathbf{2_{mono}}$ for purification and/or an X-ray crystallographic study of $\mathbf{2_{mono}}$ were unsuccessful due to its propensity to dimerize after long periods of time in concentrated solutions. This phenomenon has been observed previously by one of the authors.[16] ^{1}H NMR ($CDCl_3$, 500 MHz): δ 1.34 (s, 18H), 1.42 (s, 3H), 1.59 (s, 3H), 4.43 (t, J = 11.3 Hz, 1H), 4.98 (t, *J* = 11.4 Hz, 1H), 5.80 (m, 1H), 6.40 (dd, *J* = 16.0, 13.0 Hz, 1H), 7.37 (s, 1H), 7.56 (s, 2H), 7.61 (d, *J* = 8.6 Hz, 1H), 7.68 (d, *J* = 7.7 Hz, 1H), 7.96 (d, *J* = 8.4 Hz, 1H), 8.12 (d, *J* = 8.5 Hz, 1H), 8.41 (d, *J* = 8.8 Hz, 1H), 10.41 (d, *J* = 8.8 Hz, 1H). ^{13}C NMR ($CDCl_3$, 125 MHz): δ 14.2, 22.5, 22.7, 22.9, 23.4, 31.7, 34.3, 35.1, 47.9, 52.1, 52.9, 59.0, 59.1, 65.9, 66.3, 120.6, 121.1, 121.9, 127.6, 127.6, 127.8, 129.8, 131.0, 139.8, 142.1, 147.2, 151.3, 163.6, 170.0, 177.6, 178.7.

Synthesis of complex 3. The following reaction was performed under the strict exclusion of oxygen and moisture using an Argon filled Mbraun dry box and standard Schlenk techniques. Solvents were dried over Na metal prior to use. C_6D_6 was dried by distillation from Na/benzophenone and stored over a K° mirror in a Teflon sealed ampoule. Toluene-d_8 was distilled from sodium metal and stored over freshly activated metallic sodium in a Teflon sealed ampoule. Neutral alumina (Al_2O_3) was heated at 150 °C under high vacuum for 48 hours and used immediately.

Procedure. Charge a 20 mL scintillation vial with ^{Et}**APAQ** ligand $\mathbf{L_3}$ (30 mg, 93.0 μmol, 1 equiv.), $Pd(OAc)_2$ (21.9 mg, 97.7 μmol, 1.05 equiv.) and 2,6-di-tert-butyl-4-methylpyridine ^{tBu2}**Py** (10.4 mg, 93.0 μmol, 1 equiv.) under an argon atmosphere. Add 3 mL benzene and stir for 24 hours at room temperature. Filtrate the resulting mixture through a 3-inch Al_2O_3 pipette column. Wash the column with an additional 3 mL of benzene (eluent should become clear before the additional 3 mL finishes eluting). Concentrate the filtrate and repeat filtration through a second 3-inch alumina pipette column. ***N.B.*** *presence of any moisture during filtration causes hydrolysis of the product*. Concentration of the organic phase yields complex **3** as a light-yellow powder in 27% yield (14.9 mg, 25.1 μmol). Single crystals suitable for an X-ray diffraction study were grown in an inverted J-Young NMR tube at room temperature overnight from a saturated benzene solution layered with Bu_2O. M.P. xxxxx °C dec. ^{1}H NMR ($CDCl_3$, 500 MHz): δ 0.95 (s, 9H), 1.40 (s, 9H), 1.84 (s, 3H), 2.35 (s, 3H), 2.65 (s, 3H), 3.36-3.45 (m, 4H), 4.28 (dd, *J* = 14.34, 6.76 Hz, 1H), 4.48 (t, *J* = 8.71 Hz,1H), 4.81 (m, 1H), 5.19 (d, *J* = 10.70 Hz, 1H), 5.56 (s, 1H), 6.37 (d, *J* = 7.58 Hz, 2H), 6.55 (d, *J* = 7.09 Hz, 1H), 6.70 (t, *J* = 7.39 Hz, 1H), 6.77 (t, *J* = 7.19 Hz, 1H), 6.93-6.99 (m,

3H), 7.43 (d, *J* = 7.69 Hz, 1H), 8.59 (d, *J* = 10.67 Hz, 1H). ^{13}C NMR ($CDCl_3$, 125 MHz): δ 9.7, 22.4, 27.2, 29.3, 29.4, 31.1, 42.7, 62.7, 77.4, 80.9, 124.8, 129.8, 134.1, 145.1, 168.3, 250.9. HRMS ESI-TOF+ found m/z = xxx.xxxx, $[M + H]^+$ calculated for $[C_{31}H_{41}N_2O_3Pd]^+$ m/z = 595.2152.

Crystallographic Structure Determinations. Single-crystal X-ray structure determinations were carried out at low temperature on a Bruker P4, Platform, or Kappa diffractometer equipped with a Mo or Cu radiation source and a Bruker APEX detector. All structures were solved by direct methods with SIR 2004 or SHELXS and refined by full-matrix least-squares procedures utilizing SHELXL within the Olex 2 small-molecule solution, refinement, and analysis software package.

ASSOCIATED CONTENT

Supporting Information

The Supporting Information is available free of charge on the ACS Publications website at DOI: xxxxxxx.

Spectral data and crystallographic tables for all new compounds and cartesian coordinates (PDF).

Accession Codes

CCDC 1917901 (**1**), 1917900 (**2**), and 1917902 (**3**) contain the supplementary crystallographic data for this paper. These data can be obtained free of charge via www.ccdc.cam.ac.uk/data_request/cif, or by emailing data_request@ccdc.cam.ac.uk, or by contacting The Cambridge Crystallographic Data Centre, 12 Union Road, Cambridge CB2 1EZ, UK; fax: +44 1223 336033.

AUTHOR INFORMATION

Corresponding Author

* E-mail (GB): gbertrand@ucsd.edu
* E-mail (J-QY): yu200@scripps.edu

Present Addresses

EAR: Department of Chemistry, University of California Berkeley, Berkeley, California 94720-1460, United States
GC: School of Chemistry and Chemical Engineering, Shanghai Jiao Tong University, 800 Dongchuan Rd., Minhang District, Shanghai 200240, China

ORCID

Erik A. Romero: 0000-0002-5155-1684
Rodolphe Jazzar: 0000-0002-4156-7826
Guy Bertrand: 0000-0003-2623-2363
Jin-Quan Yu: 0000-0003-3560-5774

Notes

The authors declare no competing financial interest.

ACKNOWLEDGMENTS

This work was supported by the U.S. Department of Energy, Office of Science, Basic Energy Sciences, Catalysis Science Program, under Award No. DE-SC0009376 (GB) and xxxxxxxxxxxxx (J-QY). Thanks are due to the U.S. Department of Education for a GAANN fellowship (EAR). We further thank SIOC, Zhejiang Medicine and Pharmaron (fellowships for GC). EAR also thanks Ms. Kristen Wang for helpful discussions regarding the steric topographical analysis.

REFERENCES

(1) (a) Karimov, R. R.; Hartwig, J. F. Transition-Metal-Catalyzed Selective Functionalization of C(sp^3)–H Bonds in Natural Products. *Angew. Chem. Int. Ed.* **2018**, *57*, 4234-4241. (b) He, J.; Wasa, M.; Chan, K. S. L.; Shao, Q.; Yu, J.-Q. Palladium-Catalyzed Transformations of Alkyl C–H Bonds. *Chem. Rev.* **2017**, *117*, 8754-8786. (c) Park, Y.; Kim, Y.; Chang, S. Transition Metal-Catalyzed C–H Amination: Scope, Mechanism, and Applications. *Chem. Rev.* **2017**, *117*, 9247-9301. (d) Mkhalid, I. A. I.; Barnard, J. H.; Marder, T. B.; Murphy, J. M.; Hartwig, J. F. C–H Activation for the Construction of C–B Bonds. *Chem. Rev.* **2010**, *110*, 890-931. (e) Labinger, J. A.; Bercaw, J. E. Understanding and exploiting C–H bond activation. *Nature* **2002**, *417*, 507.

(2) (a) Woźniak, Ł.; Cramer, N. Enantioselective C H Bond Functionalizations by 3d Transition-Metal Catalysts. *Trends in Chemistry* **2019**, *online*. (b) Newton, C. G.; Wang, S.-G.; Oliveira, C. C.; Cramer, N. Catalytic Enantioselective Transformations Involving C–H Bond Cleavage by Transition-Metal Complexes. *Chem. Rev.* **2017**, *117*, 8908-8976. (c) Giri, R.; Shi, B.-F.; Engle, K. M.; Maugel, N.; Yu, J.-Q. Transition metal-catalyzed C–H activation reactions: diastereoselectivity and enantioselectivity. *Chem. Soc. Rev.* **2009**, *38*, 3242-3272.

(3) (a) Hartwig, J. F.; Larsen, M. A. Undirected, Homogeneous C–H Bond Functionalization: Challenges and Opportunities. *ACS Cent. Sci.* **2016**, *2*, 281-292. (b) Lee, M.; Sanford, M. S. Platinum-Catalyzed, Terminal-Selective C(sp^3)–H Oxidation of Aliphatic Amines. *J. Am. Chem. Soc.* **2015**, *137*, 12796-12799. (c) Newhouse, T.; Baran, P. S. If C-H Bonds Could Talk: Selective C-H Bond Oxidation. *Angew. Chem. Int. Ed.* **2011**, *50*, 3362-3374. (d) Jazzar, R.; Hitce, J.; Renaudat, A.; Sofack-Kreutzer, J.; Baudoin, O. Functionalization of Organic Molecules by Transition-Metal-Catalyzed C(sp^3)-H Activation. *Chem. Eur. J.* **2010**, *16*, 2654-2672.

(4) (a) Cabrera, P. J.; Lee, M.; Sanford, M. S. Second-Generation Palladium Catalyst System for Transannular C–H Functionalization of Azabicycloalkanes. *J. Am. Chem. Soc.* **2018**, *140*, 5599-5606. (b) Topczewski, J. J.; Cabrera, P. J.; Saper, N. I.; Sanford, M. S. Palladium-catalysed transannular C–H functionalization of alicyclic amines. *Nature* **2016**, *531*, 220. (c) Franzoni, I.; Mazet, C. Recent trends in Pd-catalyzed remote functionalization of carbonyl compounds. *Org. Biomol. Chem.* **2014**, *12*, 233-241. (d) Lyons, T. W.; Sanford, M. S. Palladium-Catalyzed Ligand-Directed C–H Functionalization Reactions. *Chem. Rev.* **2010**, *110*, 1147-1169.

(5) (a) Park, H.; Chekshin, N.; Shen, P.-X.; Yu, J.-Q. Ligand-Enabled, Palladium-Catalyzed β-C(sp^3)–H Arylation of Weinreb Amides. *ACS Cat.* **2018**, *8*, 9292-9297. (b) Fu, H.; Shen, P.-X.; He, J.; Zhang, F.; Li, S.; Wang, P.; Liu, T.; Yu, J.-Q. Ligand-Enabled Alkynylation of C(sp^3)–H Bonds with Palladium(II) Catalysts. *Angew. Chem.* **2017**, *129*, 1899-1902. (c) Wang, H.-W.; Lu, Y.; Zhang, B.; He, J.; Xu, H.-J.; Kang, Y.-S.; Sun, W.-Y.; Yu, J.-Q. Ligand-Promoted Rhodium(III)-Catalyzed ortho-C–H Amination with Free Amines. *Angew. Chem. Int. Ed.* **2017**, *56*, 7449-7453. (d) Zhu, R.-Y.; Saint-Denis, T. G.; Shao, Y.; He, J.; Sieber, J. D.; Senanayake, C. H.; Yu, J.-Q. Ligand-Enabled Pd(II)-Catalyzed Bromination and Iodination of C(sp^3)–H Bonds. *J. Am. Chem. Soc.* **2017**, *139*, 5724-5727. (e) Sun, S.-Z.; Shang, M.; Wang, H.-L.; Lin, H.-X.; Dai, H.-X.; Yu, J.-Q. Cu(II)-Mediated C(sp2)–H Hydroxylation. *J. Org. Chem.* **2015**, *80*, 8843-8848. (f) He, J.; Shigenari, T.; Yu, J.-Q. Palladium(0)/PAr3-Catalyzed Intermolecular Amination of C(sp3)□H Bonds: Synthesis of β-Amino Acids. *Angew. Chem. Int. Ed.* **2015**, *54*, 6545-6549.

(6) (a) He, J.; Shao, Q.; Wu, Q.; Yu, J.-Q. Pd(II)-Catalyzed Enantioselective C(sp^3)–H Borylation. *J. Am. Chem. Soc.* **2017**, *139*, 3344-3347. (b) Wu, Q.-F.; Shen, P.-X.; He, J.; Wang, X.-B.; Zhang, F.; Shao, Q.; Zhu, R.-Y.; Mapelli, C.; Qiao, J. X.; Poss, M. A.; Yu, J.-Q. Formation of α-chiral centers by asymmetric β-C(sp^3)–H arylation, alkenylation, and alkynylation. *Science* **2017**, *355*, 499. (c) Xiao, K.-J.; Lin, D. W.; Miura, M.; Zhu, R.-Y.; Gong, W.; Wasa, M.; Yu, J.-Q. Palladium(II)-Catalyzed Enantioselective C(sp3)–H Activation Using a Chiral Hydroxamic Acid Ligand. *J. Am. Chem. Soc.* **2014**, *136*, 8138-8142. (d) Wasa, M.; Engle, K. M.; Lin, D. W.; Yoo, E. J.; Yu, J.-Q. Pd(II)-Catalyzed Enantioselective C–H Activation of Cyclopropanes. *J. Am. Chem. Soc.* **2011**, *133*, 19598-19601.

(7) Chen, G.; Gong, W.; Zhuang, Z.; Andrä, M. S.; Chen, Y.-Q.; Hong, X.; Yang, Y.-F.; Liu, T.; Houk, K. N.; Yu, J.-Q. Ligand-accelerated

enantioselective methylene C(sp³)–H bond activation. *Science* **2016**, *353*, 1023.
(8) Yang, Y.-F.; Chen, G.; Hong, X.; Yu, J.-Q.; Houk, K. N. The Origins of Dramatic Differences in Five-Membered vs Six-Membered Chelation of Pd(II) on Efficiency of C(sp³)–H Bond Activation. *J. Am. Chem. Soc.* **2017**, *139*, 8514-8521.
(9) Frisch, M. J.; Trucks, G. W.; Schlegel, H. B.; Scuseria, G. E.; Robb, M. A.; Cheeseman, J. R.; Scalmani, G.; Barone, V.; Petersson, G. A.; Nakatsuji, H.; Li, X.; Caricato, M.; Marenich, A. V.; Bloino, J.; Janesko, B. G.; Gomperts, R.; Mennucci, B.; Hratchian, H. P.; Ortiz, J. V.; Izmaylov, A. F.; Sonnenberg, J. L.; Williams; Ding, F.; Lipparini, F.; Egidi, F.; Goings, J.; Peng, B.; Petrone, A.; Henderson, T.; Ranasinghe, D.; Zakrzewski, V. G.; Gao, J.; Rega, N.; Zheng, G.; Liang, W.; Hada, M.; Ehara, M.; Toyota, K.; Fukuda, R.; Hasegawa, J.; Ishida, M.; Nakajima, T.; Honda, Y.; Kitao, O.; Nakai, H.; Vreven, T.; Throssell, K.; Montgomery Jr., J. A.; Peralta, J. E.; Ogliaro, F.; Bearpark, M. J.; Heyd, J. J.; Brothers, E. N.; Kudin, K. N.; Staroverov, V. N.; Keith, T. A.; Kobayashi, R.; Normand, J.; Raghavachari, K.; Rendell, A. P.; Burant, J. C.; Iyengar, S. S.; Tomasi, J.; Cossi, M.; Millam, J. M.; Klene, M.; Adamo, C.; Cammi, R.; Ochterski, J. W.; Martin, R. L.; Morokuma, K.; Farkas, O.; Foresman, J. B.; Fox, D. J. Wallingford, CT, 2016.
(10) (a) Becke, A. D. Density-functional thermochemistry. III. The role of exact exchange. *J. Chem. Phys.* **1993**, *98*, 5648-5652. (b) Lee, C.; Yang, W.; Parr, R. G. Development of the Colle-Salvetti correlation-energy formula into a functional of the electron density. *Phys. Rev. B* **1988**, *37*, 785-789.
(11) Andrae, D.; Häußermann, U.; Dolg, M.; Stoll, H.; Preuß, H. Energy-adjustedab initio pseudopotentials for the second and third row transition elements. *Theor Chim Acta* **1990**, *77*, 123-141.
(12) (a) Petersson, G. A.; Al-Laham, M. A. A complete basis set model chemistry. II. Open-shell systems and the total energies of the first-row atoms. *J. Chem. Phys.* **1991**, *94*, 6081-6090. (b) Petersson, G. A.; Bennett, A.; Tensfeldt, T. G.; Al-Laham, M. A.; Shirley, W. A.; Mantzaris, J. A complete basis set model chemistry. I. The total energies of closed-shell atoms and hydrides of the first-row elements. *J. Chem. Phys.* **1988**, *89*, 2193-2218.
(13) (a) Grimme, S.; Antony, J.; Ehrlich, S.; Krieg, H. A consistent and accurate ab initio parametrization of density functional dispersion correction (DFT-D) for the 94 elements H-Pu. *J. Chem. Phys.* **2010**, *132*, 154104. (b) Grimme, S. Semiempirical GGA-type density functional constructed with a long-range dispersion correction. *J. Comput. Chem.* **2006**, *27*, 1787-1799. (c) Grimme, S. Accurate description of van der Waals complexes by density functional theory including empirical corrections. *J. Comput. Chem.* **2004**, *25*, 1463-1473.
(14) Legault, C. Y. CYLView, 1.0b; Université de Sherbrooke: Canada, 2009; http://www.cylview.org.
(15) (a) Cabrera-Pardo, J. R.; Trowbridge, A.; Nappi, M.; Ozaki, K.; Gaunt, M. J. Selective Palladium(II)-Catalyzed Carbonylation of Methylene β-C–H Bonds in Aliphatic Amines. *Angew. Chem. Int. Ed.* **2017**, *56*, 11958-11962. (b) Landstrom, E. B.; Handa, S.; Aue, D. H.; Gallou, F.; Lipshutz, B. H. EvanPhos: a ligand for ppm level Pd-catalyzed Suzuki–Miyaura couplings in either organic solvent or water. *Green Chemistry* **2018**, *20*, 3436-3443. (c) Paavola, S.; Zetterberg, K.; Privalov, T.; Csöregh, I.; Moberg, C. Aerobic Oxidation of 1-Phenylethanol Catalyzed by Palladaheterocycles. *Adv. Synth. Catal.* **2004**, *346*, 237-244. (d) Yao, J.; Feng, R.; Wu, Z.; Liu, Z.; Zhang, Y. Palladium-Catalyzed Decarboxylative Coupling of α-Oxocarboxylic Acids with C(sp²)-H of 2-Aryloxypyridines. *Adv. Synth. Catal.* **2013**, *355*, 1517-1522. (e) Yao, Q.; Zabawa, M.; Woo, J.; Zheng, C. Carbocyclic Carbene Ligands Derived from Aromatic Nitrones: Formation and Catalytic Activity of Their Pd(II) Complexes. *J. Am. Chem. Soc.* **2007**, *129*, 3088-3089.
(16) Romero, E. A.; Olsen, P. M.; Jazzar, R.; Soleilhavoup, M.; Gembicky, M.; Bertrand, G. Spectroscopic Evidence for a Monomeric Copper(I) Hydride and Crystallographic Characterization of a Monomeric Silver(I) Hydride. *Angew. Chem. Int. Ed.* **2017**, *56*, 4024-4027.
(17) Falivene, L.; Credendino, R.; Poater, A.; Petta, A.; Serra, L.; Oliva, R.; Scarano, V.; Cavallo, L. SambVca 2. A Web Tool for Analyzing Catalytic Pockets with Topographic Steric Maps. *Organometallics* **2016**, *35*, 2286-2293.
(18) Clavier, H.; Nolan, S. P. Percent buried volume for phosphine and N-heterocyclic carbene ligands: steric properties in organometallic chemistry. *Chem. Commun.* **2010**, *46*, 841-861.
(19) Knowles, R. R.; Jacobsen, E. N. Attractive noncovalent interactions in asymmetric catalysis: Links between enzymes and small molecule catalysts. *Proc. Natl. Acad. Sci.* **2010**, *107*, 20678.

Authors are required to submit a graphic entry for the Table of Contents (TOC) that, in conjunction with the manuscript title, should give the reader a representative idea of one of the following: A key structure, reaction, equation, concept, or theorem, etc., that is discussed in the manuscript. Consult the journal's Instructions for Authors for TOC graphic specifications.

Insert Table of Contents artwork here